Proceedings of the 1998 IEEE
International Conference on Control Applications
Trieste, Italy 1-4 September 1998

WP03

Decentralized Variable Structure Control for Active Suspensions Based on a Full-Car Model

Jong H. Park and Young S. Kim
School of Mechanical Engineering
Hanyang University
Seoul, 133-791, Korea
jong.park@ieee.org

Abstract

A decentralized variable structure controller (DVSC) is designed for active suspensions of vehicles based on a 7-degree-of-freedom full-car model. Its nominal stability and stability robustness to parameter variations are assured through stability analysis. The performance of the DVSC is compared with that of a LQR controller in computer simulations. From the simulations, it is found that active suspensions with the DVSC reduce the acceleration of the sprung mass in the heaving, rolling, and pitching directions when the car is driven on a normal road or through an unequal bump. The suspension stroke and road holding capability are also compared under the assumption of equal power consumption.

1. INTRODUCTION

Over recent years, designers of modern vehicle suspensions have begun to seriously consider the use of active suspensions due to their potential to improve driver's ride quality, structural constraint, and road holding capability. Many studies on active suspensions [1, 2], however, have been devoted to simplified 2-degree-of-freedom quarter-car models, with only few studies about the overall motion control of the full vehicle.

Lately, some researches [3, 4, 5] have been done to control rolling and pitching as well as vertical acceleration of the chassis, but they lacked the robustness to system parameter changes.

Sliding mode controllers have the advantage of overcoming system parameter variations [6, 7, 8]. However, it is difficult to design a satisfactory sliding-mode controller for a full-car model using conventional methods, due to the fact that the procedure to derive its discontinuity gains is complexly coupled, resulting in a very complex sliding-mode control law.

However, it is possible to solve for simple discontinuity gains if the sliding mode control called the "decentralized variable structure control (DVSC)", based on a regular state-space form of the plant dynamics, is used [6, 7].

This paper proposes a design procedure for DVSC for active suspensions which is robust to system parameter variations, as well as extending the vehicle model to a more complete one, based on a rigid sprung mass and four wheel-axle assemblies.

Section 2 describes the full-car model based on 7 degrees of freedom. Section 3 includes explanations on DVSC and its design procedure as well as a brief review of a LQG design. The performance of the DVSC and the LQG designs is compared in computer simulations in section 4 under the assumption of an equal level of actuator power. Section 4 concludes.

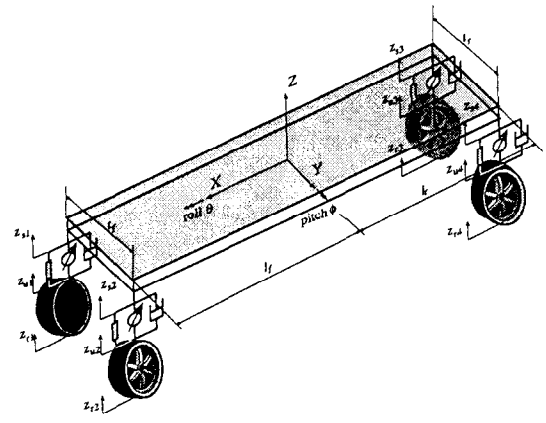

Figure 1: Schematic diagram of the full-car model.

2. VEHICLE MODELING

The vehicle model considered in this paper comprises five parts: the chassis (sprung mass) and four wheel-axle assemblies (unsprung masses) as shown in Fig. 1. The sprung mass is assumed to be rigid and has freedom of motion in the vertical, pitch, and roll directions. Each of the unsprung masses has freedom of motion in the vertical direction. Thus, the full-car model has 7 degrees of freedom. Each suspension consists of a linear spring, a damper, and an actuator to generate pushing-force between the chassis and each axle. The dynamics of the actuators are assumed to be negligible compared to the response of suspensions.

The governing equations of motion for the full-car model are:

$$M_s\ddot{p} = GB_s(\dot{z}_u - \dot{z}_s) + Gk_{sr}(z_u - z_s) + Gu \quad (1)$$

$$M_u\ddot{z}_u = B_s(\dot{z}_s - \dot{z}_u) + K_{ss}(z_s - z_u) + K_t(z_r - z_u) - u \quad (2)$$

where

$$p = [z_c \quad \theta \quad \phi]^T \in \mathbb{R}^3,$$
$$z_j = [z_{j1} \quad z_{j2} \quad z_{j3} \quad z_{j4}]^T \in \mathbb{R}^4, \; j = u, s, r$$
$$u = [u_1 \quad u_2 \quad u_3 \quad u_4]^T \in \mathbb{R}^4,$$

where z_c, θ, and ϕ denote the vertical displacement at the center of gravity, the roll angle, and the pitch angle, respectively, of the sprung mass; and z_{ui}, z_{si}, z_{ri}, and u_i denote the vertical displacement of the unsprung mass, the vertical displacement of the sprung mass, the vertical displacement of the road, and the pushing force generated by the actuator, respectively, at suspension i. The matrices that appear in Eqs. (1) and (2) are expressed as

$$M_s = \text{diag}(m_s, I_\theta, I_\phi), \quad M_u = \text{diag}(m_f, m_f, m_r, m_r),$$
$$B_s = \text{diag}(b_f, b_f, b_r, b_r), \quad K_{ss} = \text{diag}(k_f, k_f, k_r, k_r),$$
$$K_t = \begin{bmatrix} k_{tf} & 0 & 0 & 0 \\ 0 & k_{tf} & 0 & 0 \\ 0 & 0 & k_{tr} & 0 \\ 0 & 0 & 0 & k_{tr} \end{bmatrix},$$
$$K_{sr} = \begin{bmatrix} k_f + r_f/2 & -r_f/2 & 0 & 0 \\ -r_f/2 & k_f + r_f/2 & 0 & 0 \\ 0 & 0 & k_r + r_r/2 & -r_r/2 \\ 0 & 0 & -r_r/2 & k_r + r_r/2 \end{bmatrix},$$
$$\text{and} \quad G = \begin{bmatrix} 1 & 1 & 1 & 1 \\ -t_f & t_f & -t_r & t_r \\ -l_f & -l_f & l_r & l_r \end{bmatrix}.$$

where all the parameters are explained in Table 1 along with their numerical values used in the later simulations.

And z_s and p have a kinematic relationship of

$$z_s = G^T p. \tag{3}$$

Substituting Eq. (3) into Eqs. (1) and (2),

$$M\ddot{z} + B_z\dot{z} + K_a z - K_b z_r = G_a u \tag{4}$$

where

$$z = [p^T \quad z_u^T]^T \in \mathbb{R}^7$$

and all the matrices are of appropriate dimensions:

$$M = \begin{bmatrix} M_s & 0 \\ 0 & M_u \end{bmatrix}, \quad B_z = \begin{bmatrix} GB_sG^T & -GB_s \\ -B_sG^T & B_s \end{bmatrix}$$
$$K_a = \begin{bmatrix} GK_{sr}G^T & -GK_{sr} \\ -K_{ss}G^T & K_t + K_{ss} \end{bmatrix}, \quad K_b = \begin{bmatrix} 0 \\ K_t \end{bmatrix}, \quad \text{and}$$
$$G_a = \begin{bmatrix} G \\ -I \end{bmatrix}.$$

Equation (4) can be represented as a state-space form of

$$\dot{x} = Ax + Bu + Fz_r \tag{5}$$

Table 1: Parameters of the vehicle model used.

Parameters (Symbols)	Values
sprung mass (m_s)	1,460 kg
front unsprung mass (m_f)	40 kg
rear unsprung mass (m_r)	35.5 kg
roll moment of inertia of the sprung mass (I_θ)	460 kg·m^2
pitch moment of inertia of the sprung mass (I_ϕ)	2,460 kg·m^2
front suspension damping rate (b_f)	1,290 N·s/m
rear suspension damping rate (b_r)	1,620 N·s/m
front suspension stiffness (k_f)	19,960 N/m
rear suspension stiffness (k_r)	17,500 N/m
front antiroll-bar stiffness (r_f)	19,200 N·rad/m
rear antiroll-bar stiffness (r_r)	9,600 N·rad/m
front tire stiffness (k_{tf})	175,500 N/m
rear tire stiffness (k_{tr})	175,500 N/m
half the distance between the front wheels (t_f)	0.761 m
half the distance between the rear wheels (t_r)	0.755 m
distance between the c.g. and the front axle (l_f)	1.011 m
distance between the c.g. and the rear axle (l_r)	1,803 m

where

$$x = [z^T \quad \dot{z}^T]^T \in \mathbb{R}^{14}$$
$$A = \begin{bmatrix} 0 & I \\ -M^{-1}K_a & -M^{-1}B_z \end{bmatrix}, \quad B = \begin{bmatrix} 0 \\ M^{-1}G_a \end{bmatrix}, \quad \text{and}$$
$$F = \begin{bmatrix} 0 \\ M^{-1}K_b \end{bmatrix}.$$

3. CONTROLLER DESIGN

3.1. Decentralized Variable Structure Controller (DVSC) Design

In order to apply the sliding mode control on the suspension system, it is required to transform the original plant model of Eq. (5) to a regular form [6, 7] of

$$\dot{\gamma}_1 = f_1(\gamma)$$
$$\dot{\gamma}_2 = f_2(\gamma) + u \tag{6}$$

where u is the control input, $\gamma = [\gamma_1^T \quad \gamma_2^T]^T \in \mathbb{R}^{14}$, $\gamma_1 \in \mathbb{R}^{10}$, and $\gamma_2 \in \mathbb{R}^4$, with a linear transformation $T \in \mathbb{R}^{14\times 14}$, i.e.,

$$\gamma = Tx. \tag{7}$$

This requirement is expressed as

$$TB = [0_{4,10} \quad I_4]^T, \tag{8}$$

where I_4 denotes a 4-by-4 identity matrix.

Transformation matrices that satisfy both Eq. (7) and Eq. (8) can be expressed as

$$T = B_\gamma B^+ + Q^T \tag{9}$$

where $B_\gamma = [0_{4,10} \quad I_4]^T$ and B^+ is the Moor-Penrose inverse of matrix B. The columns of Q spans the null space of B^T.

By substituting Eq. (9) into Eq. (5), a regular form is obtained as

$$\dot{\gamma} = A_\gamma \gamma + B_\gamma u + F_\gamma z_r \tag{10a}$$

where

$$A_\gamma = TAT^{-1}, \quad B_\gamma = TB, \quad F_\gamma = TF$$

or

$$\begin{bmatrix} \dot{\gamma}_1 \\ \dot{\gamma}_2 \end{bmatrix} = \begin{bmatrix} A_{11} & A_{12} \\ A_{21} & A_{22} \end{bmatrix} \begin{bmatrix} \gamma_1 \\ \gamma_2 \end{bmatrix} + \begin{bmatrix} 0_{10,4} \\ I_4 \end{bmatrix} u + \begin{bmatrix} F_1 \\ F_2 \end{bmatrix} z_r \tag{10b}$$

We begin the design of the sliding mode controller by defining a sliding surface as

$$\sigma = S\gamma = [S_1 \quad S_2] \begin{bmatrix} \gamma_1 \\ \gamma_2 \end{bmatrix} = S_1\gamma_1 + S_2\gamma_2 \tag{11}$$

where $\sigma \in \mathbb{R}^4$, $S_1 \in \mathbb{R}^{4\times 10}$, and nonsingular $S_2 \in \mathbb{R}^{4\times 4}$.

If the system is on the sliding surface,

$$\sigma = 0, \tag{12}$$

and, thus

$$\gamma_2 = -S_2^{-1} S_1 \gamma_1 = -F_b \gamma_1, \tag{13}$$

where $F_b = S_2^{-1} S_1$.

Substituting Eq. (13) into Eq. (10b),

$$\begin{aligned} \dot{\gamma}_1 &= A_{11}\gamma_1 + A_{12}\gamma_2 + F_1 z_r \\ &= (A_{11} - A_{12}F_b)\gamma_1 + F_1 z_r \end{aligned} \tag{14}$$

The reduced-order dynamics of Eq. (14) on the sliding surface is independent of control input u and exhibits a state-feedback structure where F_b and A_{12} represent a "state feedback matrix" and an "input" matrix, respectively.

If system (A_{11}, A_{12}) is stabilizable, it is possible to find the optimal F_b, a "feedback control gain", that minimizes performance index

$$J = \int_0^\infty \gamma_1^T Q \gamma_1 + \gamma_2^T R \gamma_2 + \gamma_1^T N \gamma_2 \, dt \tag{15}$$

where the lower limit of the integration refers to the initiation of sliding; $Q \geq 0$, $R > 0$. This optimal F_b maximizes index J and asymptotically stabilizes γ_1.

Note that it would be difficult to find appropriate matrices in Eq. (15) for desirable performance of the system since γ's are not directly associated with physical state variables. Therefore, it is desirable to find perform indices expressed in terms of physical state variables.

By using the relation of

$$x = T^{-1}\gamma = [W_1 \quad W_2] \begin{bmatrix} \gamma_1 \\ \gamma_2 \end{bmatrix} = W_1\gamma_1 + W_2\gamma_2 \tag{16}$$

a cost index which depends on the physical state variables can be expressed in terms of state variables of the regular form. Suppose a cost function is defined as an integral of a quadratic function of x. Then, it can be expressed in the form of Eq. (15) as

$$\begin{aligned} J &= \int_0^\infty x^T Q_s x \, dt \\ &= \int_0^\infty (\gamma_1^T W_1^T Q_s W_1 \gamma_1 + 2\gamma_1^T W_1^T Q_s W_2 \gamma_2 \\ &\quad + \gamma_2^T W_2^T Q_s W_2 \gamma 2) \, dt \end{aligned} \tag{17}$$

where $Q_s > 0$.

For the simplicity, S_2 is selected as

$$S_2 = I_4,$$

resulting in simplified switching matrix

$$S = [F_b \quad I_4]. \tag{18}$$

From Eqs. (10b), (11), and (18),

$$\begin{aligned} \dot{\sigma} &= F_b\dot{\gamma}_1 + \dot{\gamma}_2 \\ &= F_b(A_{11}\gamma_1 + A_{12}\gamma_2 + F_1 z_r) \\ &\quad A_{21}\gamma_1 + A_{22}\gamma_2 + u + F_2 z_r. \end{aligned} \tag{19}$$

Thus, the equivalent control, which satisfies $\dot{\sigma} = 0$, becomes

$$\begin{aligned} u_{eq} &= -F_b(A_{11}\gamma_1 + A_{12}\gamma_2 + F_1 z_r) \\ &\quad - A_{21}\gamma_1 - A_{22}\gamma_2 - F_2 z_r \end{aligned} \tag{20}$$

In order to take care of uncertainty of the system, the actual control input is modified as

$$u = \hat{u}_{eq} - H \cdot \mathrm{sgn}(\sigma) \tag{21}$$

where

$$H = \mathrm{diag}(h_i),$$

$$\mathrm{sgn}(\sigma) = [\mathrm{sgn}(\sigma_1) \quad \mathrm{sgn}(\sigma_2) \quad \mathrm{sgn}(\sigma_3) \quad \mathrm{sgn}(\sigma_4)]^T,$$

and

$$\begin{aligned} \hat{u}_{eq} &= -F_b(\hat{A}_{11}\gamma_1 + \hat{A}_{12}\gamma_2 + \hat{F}_1 z_r) \\ &\quad - \hat{A}_{21}\gamma_1 - \hat{A}_{22}\gamma_2 - \hat{F}_2 z_r \end{aligned} \tag{22}$$

where $\hat{u}_{eq}$ is the equivalent control which is based on estimates of system parameters rather than actual values. Term $H \cdot \mathrm{sgn}(\sigma)$

represents discontinuous control input and makes the sliding mode controller robust to plant parameter variations.

In order to prove the stability of Eq. (21), a Lyapunov function candidate is selected as

$$V = \frac{1}{2}\sigma^T\sigma. \tag{23}$$

By differentiating Eq. (23), and using Eqs. (10b), (11), and (18),

$$\begin{aligned}\dot{V} &= \sigma^T(F_b\dot{\gamma}_1 + \dot{\gamma}_2)\\ &= \sigma^T\Big\{F_b(\tilde{A}_{11}\gamma_1 + \tilde{A}_{12}\gamma_2 + \tilde{F}_1 z_r)\\ &\quad + \tilde{A}_{21}\gamma_1 + \tilde{A}_{22}\gamma_2 + \tilde{F}_2 z_r\Big\} - \sum_{i=1}^{4} h_i|\sigma_i|\end{aligned} \tag{24}$$

where $\tilde{A}_{ij} = A_{ij} - \hat{A}_{ij}$ for $i, j = 1, 2$.

If the components of diagonal matrix H are selected such that

$$\begin{aligned}h_i \geq \eta_i &+ \|F_b\tilde{A}_{11} + \tilde{A}_{21}\|\,|\gamma_1| + \|F_b\tilde{A}_{12} + \tilde{A}_{22}\|\,|\gamma_2|\\ &+ \|F_b\tilde{F}_1 + \tilde{F}_2\|\,|z_r|,\end{aligned} \tag{25}$$

Eq. (24) results in

$$\dot{V} \leq -\sum_{i=1}^{4} \eta_i|\sigma_i|. \tag{26}$$

Typically, the signum function in Eq. (3.1.) can be replace by the saturation function in order to eliminate the chattering effect, and the following control input is used for the later simulations.

$$\begin{aligned}u = &-F_b(\hat{A}_{11}\gamma_1 + \hat{A}_{12}\gamma_2 + \hat{F}_1 z_r) - \hat{A}_{21}\gamma_1\\ &- \hat{A}_{22}\gamma_2 - \hat{F}_2 z_r - H\cdot\mathrm{sat}(\sigma/\Phi)\end{aligned} \tag{27}$$

where Φ is the thickness of the boundary layer and

$$\mathrm{sat}(x) = \begin{cases} 1 & \text{if } x \geq 1,\\ x & \text{if } -1 < x < 1,\\ -1 & \text{if } x \leq -1.\end{cases}$$

3.2. LQR Design

The road/terrain irregularities can be modeled as the output of a linear shaping filter with an input of white noise. Here, the filter is modeled as a first-order system [1] as

$$\dot{z}_r + \alpha z_r = w \tag{28}$$

where w is the white noise and α is the product of the road type coefficient and the vehicle speed. If the state vector is defined as $x_s = [x^T \quad z_r^T]^T$, the augmented state-space representation of the plant becomes, from Eqs. (5) and (28),

$$\dot{x}_s = A_s x_s + B_s u + F_s w \tag{29}$$

Table 2: Weighting factors of optimal cost function.

ρ_1	ρ_2	ρ_3	ρ_4	ρ_5	ρ_6
1×10^6	3×10^5	3×10^5	1×10^8	1×10^8	1

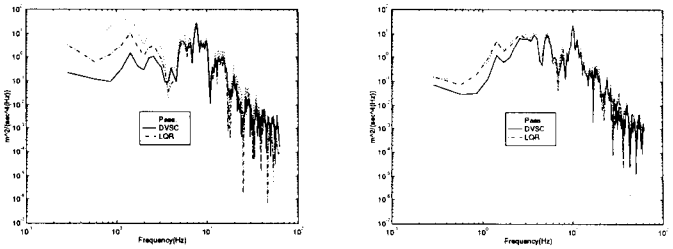

(a) (b)

Figure 2: Power spectral densities of the heaving acceleration (a); and the pitching angular acceleration (b).

where

$$A_s = \begin{bmatrix} A & F \\ 0 & -\alpha I\end{bmatrix}, \quad B_s = \begin{bmatrix} B \\ 0\end{bmatrix}, \quad F_s = \begin{bmatrix} 0 \\ I\end{bmatrix}$$

Then, the LQR controller is designed to minimize a cost function of chassis accelerations, suspension deflections and tire deflections represented by

$$\begin{aligned}J = \lim_{t\to\infty}\frac{1}{t}E\Big\{\int_0^t\Big(&\rho_1\ddot{z}^2 + \rho_2\ddot{\theta}^2 + \rho_3\ddot{\phi}^2 + \rho_4\sum_{i=1}^{4}(z_{si} - z_{ui})^2\\ &+ \rho_5\sum_{i=1}^{4}(z_{ui} - z_{ri})^2 + \rho_6\sum_{i=1}^{4}u_i^2\Big)dt\Big\}\end{aligned} \tag{30}$$

where the values of weighting factors are shown on Table 2.

4. SIMULATIONS

For the simulations of active suspension control, two types of road inputs are used to measure the responses of the vehicle over a specific band of frequencies [9] and the peak values of the responses in time domain. For all simulations, the rear vehicle input is a delayed version of that at the front wheel.

In the first simulation, the car is driven at 80 km/hr on a normal road. The power spectral densities (PSDs) of the heaving acceleration, the pitching angular acceleration, the suspension deflection of the front left wheel, and the tire deflection of the rear right wheel are shown in Figs. 2 and 3. Figure 2 shows that the DVSC exhibits a smaller level of heaving acceleration and pitching angular acceleration than that of the LQR design for the most of the frequency range. As far as the rattle space is concerned, the DVSC also shows a better performance than the LQR above 0.5 Hz. At the low frequency range, the DVSC also shows remarkably small level in tire deflection. The power consumption level of the DVSC suspension is almost identical to that of the LQR suspension.

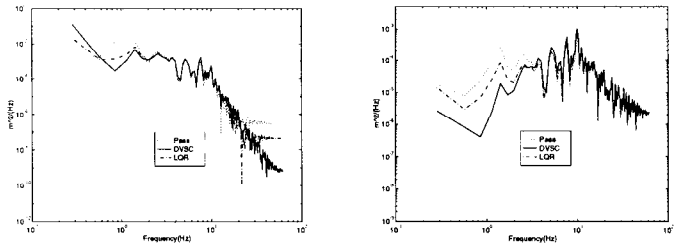

(a) (b)

Figure 3: Power spectral densities of the rattle space of the front left wheel (a); and the tire deflection of the rear right wheel (b).

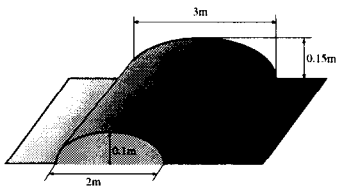

Figure 4: Bumper profile

In the second simulation, the car is driven at 35 km/hr on an unequal bumper whose profile is shown in Fig. 4. The heaving acceleration, the rolling angular velocity, the pitching angular velocity of the chassis, and the suspension deflection of the front left wheel are shown in Fig. 5. The DVSC and LQR exhibit almost identical peak levels in the heaving acceleration and the rolling rate. But the DVSC has a smaller settling time than the LQR. The pitching rate of the chassis and the rattle space are considerably smaller for the DVSC.

In the third simulation, the response and the stability of the vehicle is measured when the plant parameter variations occur. It is assumed that the mass of the chassis changes $\pm 15\%$ from its nominal value and that other parameters such as unsprung masses, moment of inertia of the sprung mass, suspension damping rate, suspension spring stiffness, and anti-roll bar rate also vary from their nominal values. When the normal road input and bumper input are used, the responses of the vehicle are almost the same as those of the nominal plant.

5. CONCLUSIONS

A decentralized variable structure controller (DVSC) is designed for a full-car model using a plant transformation to a regular form. In designing the sliding surface, the new method minimizing the performance index, which is the function of the original state is used. In order to evaluate the performance of the suspension, two simulation tests are performed: driving on a regular road and driving on a bumper. Performance evaluations are made in terms of the chassis acceleration, the rattle space and the tire deflection as well as the power consumed. For the nominal plant, the suggested DVSC shows a better performance than that of the LQR. The stability robustness to the system parameter variations is also assured.

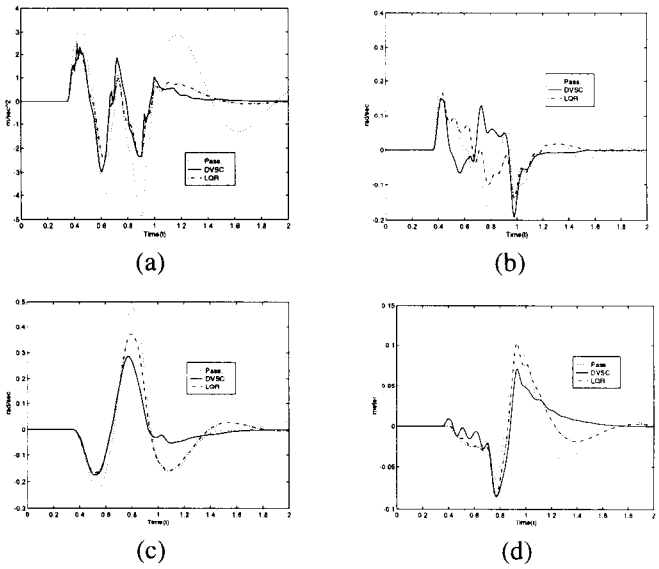

(a) (b)

(c) (d)

Figure 5: (a) Heaving acceleration of the chassis; (b) Rolling rate of the chassis; (c) Pitching rate of the chassis; and (d) Suspension deflection of the rear right wheel.

References

[1] A. Hac, "Adaptive control of vehicle suspensions," *Vehicle System Dynamics*, vol. 16, pp. 57–74, 1987.

[2] C. Yue, T. Butsuen, and J. K. Hedrick, "Alternative control laws for automotive active suspensions," *Journal of Dynamic Systems, Measurement, and Control*, vol. 111, pp. 286–291, 1989.

[3] *Application of the LQG Approach to Design of an Automotive Suspension for Three-Dimensional Vehicle Models*, 1988.

[4] D. A. Crolla and M. B. A. Abdel-Hady, "Active suspension control: Performance comparisons using control laws applied to a full vehicle model," *Vehicle System Dynamics*, vol. 20, pp. 107–120, 1991.

[5] I. Cech, "A full-car roll model of a vehicle with controlled suspension," *Vehicle System Dynamics*, vol. 23, pp. 467–480, 1994.

[6] G. P. Matthews and R. A. DeCarlo, "Decentralized tracking for a class of interconnected nonlinear systems using variable structure control," *Automatica*, vol. 24, no. 2, pp. 187–193, 1988.

[7] R. A. DeCarlo, S. H. Zak, and S. V. Drakunov, "Variable structure, sliding-mode controller design," in *Control Handbook* (W. S. Levine, ed.), CRC Press, 1996.

[8] J.-J. E. Slotine and W. Li, *Applied Nonlinear Control*. Prentice Hall, 1991.

[9] T. D. Gillespie, *Fundamentals of Vehicle Dynamics*. Society of Automotive Engineers, 1992.